焊接热输入对 X100管线钢粗晶区组织及性能的影响

张骁勇[1,2], 高惠临[2], 庄传晶[3], 吉玲康[3]
(1. 西安建筑科技大学 材料科学与工程学院, 西安 710048; 2. 西安石油大学 材料科学与工程学院, 西安 710065;
3. 中国石油天然气集团公司 管材研究所, 西安 710065)

摘 要: 采用热模拟技术、显微分析方法和力学性能测试等手段, 对 X100管线钢在不同焊接热输入下粗晶区的组织及性能的变化规律进行了研究. 结果表明, 随着焊接热输入的增加, X100管线钢的强韧性降低. 当热输入为 10 kJ/cm左右时, 焊接粗晶热影响区的显微组织以贝氏体铁素体和粒状贝氏体为主, 这种组织赋予材料以最佳的强韧性水平; 当热输入为 20 kJ/cm左右时, 焊接粗晶热影响区的显微组织以粒状贝氏体和准多边形铁素体为主, 材料有较好的强韧配合; 而当热输入大于 30 kJ/cm时, 由于多边形铁素体增多, 材料的强韧性降低. 因此可将 10~20 kJ/cm作为 X100管线钢的推荐热输入.

关键词: X100管线钢; 焊接热输入; 组织; 性能
中图分类号: TG142.1 文献标识码: A 文章编号: 0253-360X(2010)03-0029-04


张骁勇

0 序 言

X100是超高强度管线钢中的一种典型钢种. 采用 X100作为高压、大流量天然气输送管线管材, 具有较大的经济效益. 资料显示[1,2], 在油气管道建设中, 采用 X80代替 X70, 可降低成本 7%; 采用 X100代替 X70, 则可降低成本 30%. 所以 X100管线钢的研究和开发, 日益受到人们的关注. X100是一种新型的微合金化管线钢, 在国内外的研究历史不长. 在已有的文献中[3-5], 多限于管线钢钢板性能的研究, 对 X100管线钢在焊接热过程中组织及性能的特征及其变化规律却知之不多. 焊接热影响区粗晶区是整个焊接接头中性能最为薄弱的区域, 因此研究 X100管线钢在不同焊接热输入条件下的粗晶区组织及性能的变化规律及其焊接脆化的特征, 对掌握 X100管线钢焊接冶金的基本规律和推动 X100管线钢的工业应用具有重要的意义.

1 试验方法

试验用 X100管线钢板厚度为 14.3 mm, 化学成分见表 1, 力学性能见表 2, 其基本金相组织为针状铁素体.

表 1 X100的化学成分(质量分数, %)
Table 1 Chemical composition of X100 pipeline steel

C	Si	Mn	P	S	Cr	Mo
0.05	0.25	2.00	0.012	0.0032	0.33	0.33
Ni	Nb	V	Ti	Cu	Al	Fe
0.46	0.055	0.007	0.022	0.20	0.046	余量

表 2 X100的常规力学性能
Table 2 Mechanical properties of X100 pipeline steel

屈服强度 R_{eL}/MPa	抗拉强度 R_m/MPa	断后伸长率 A(%)	屈强比 R_{eL}/R_m	冲击吸收功 A_{KV}/J
730	805	20.5	0.91	191

采用热模拟试验获取 X100管线钢在不同焊接热输入条件下粗晶热影响区(coarse grain heat affect zone, CGHAZ)的组织结构. 热模拟试验在 Gleeble 1500型热模拟机上进行, 热模拟参数如表 3所示. 其中热循环的几种 $t_{8/5}$覆盖了石油、天然气输送钢管在制管焊接和野外施工焊接过程中所采用的不同焊接热输入下的冷却参数.

热模拟试样分别采用 ϕ10 mm×65 mm和 10.5 mm×10.5 mm×55 mm的初始试样, 试样于板厚中部(沿板厚方向两面对称加工)横向截取. 热模拟试验后再将试样加工 ϕ5 mm×25 mm的标准比例拉伸试样和 10 mm×10 mm×55 mm的标准 Charpy冲击试样, 沿板厚方向开制 V形缺口. 拉伸试验在

收稿日期: 2009-04-09
基金项目: 国家自然科学基金资助项目(50874090)

表 3 X100焊接粗晶影响区热模拟参数

Table 3 Thermal simulation parameters for CGHAZ

热输入 E/(kJ·cm^{-1})	加热速度 v/(℃·s^{-1})	峰值温度 T/℃	冷却时间 $t_{8/5}$/s	高温停留时间 t_H/s	
				900 ℃	1 100 ℃
10	130	1 300	5	3.62	2.95
15	130	1 300	10	5.43	3.60
20	130	1 300	20	10.86	7.20
30	130	1 300	40	21.71	14.41
40	130	1 300	70	38.00	25.23
50	130	1 300	100	54.28	36.03

MTS-880型万能试验机上进行;冲击试验在 JBC-300电子测力冲击试验机上进行.

光学金相试样经机械抛光后以 3%硝酸酒精溶液进行腐蚀,在 RECHART MEF3A光学显微镜下观察. TEM试样经机械减薄至 50 μm后,在双喷电解装置上以 10%高氯酸 +90%醋酸溶液进行双喷,在 JEM 200CX透射电子显微镜上观察. SEM试验在 TESLA-BS-300型扫描电子显微镜上进行.

2 试验结果及分析

2.1 力学性能特征

2.1.1 强塑性

X100焊接粗晶热影响区的强塑性与焊接热输入的关系如图 1所示. 从图中可以看出,随着热输入的增加,屈服强度和抗拉强度降低,断后伸长率略有变化. 在低的焊接热输入条件下可获得高的强度水平.

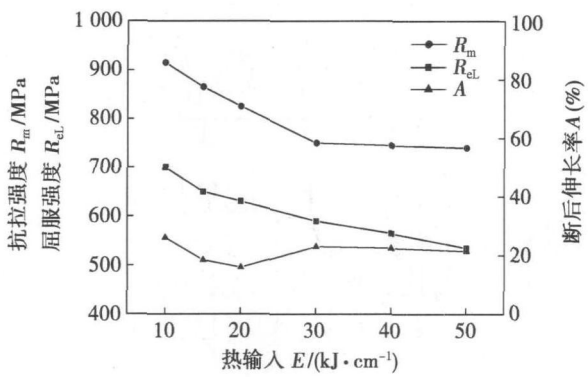

图 1 X100在不同热输入下的拉伸力学性能

Fig. 1 Tensile mechanical property of X100 at different heat inputs

2.1.2 冲击吸收功

在不同焊接热输入条件下, X100焊接粗晶热影响区在 -20 ℃时的夏比冲击吸收功变化规律如图 2所示.

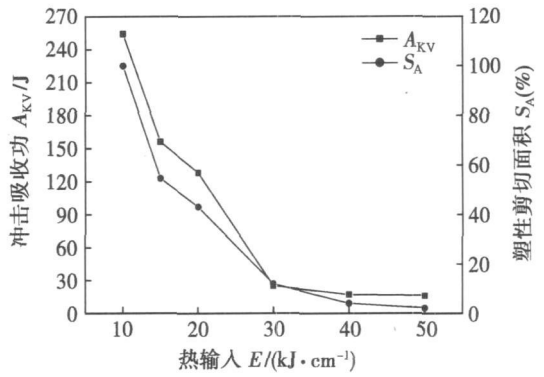

图 2 X100在不同热输入下的冲击吸收功(-20 ℃)

Fig. 2 Impact absorption energy of X100 at different heat inputs(-20 ℃)

试验结果表明, X100 CGHAZ的冲击吸收功随着热输入的增加而降低. 当热输入在 10~20 kJ/cm范围内, CGHAZ的韧性符合工程要求. 当热输入超过 20 kJ/cm时, CGHAZ的韧性明显降低,表现为焊接局部脆化.

为了研究 X100 CGHAZ的韧脆转变能力,测试了 X100 CGHAZ在热输入为 10 kJ/cm下的系列温度冲击吸收功. 试验结果如图 3所示. 试验结果表明,在不同的试验温度下,焊接粗晶热影响区的韧性变化不大,具有优良的韧脆转变能力.

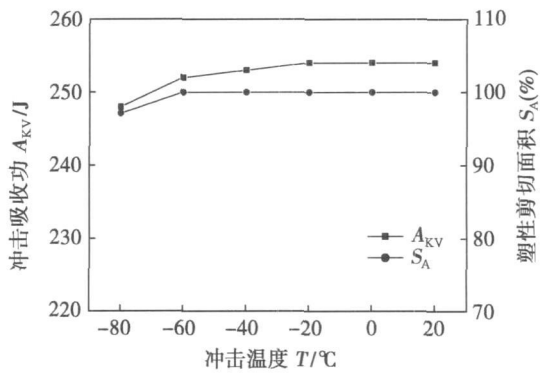

图 3 E=10 kJ/cm时 CGHAZ系列冲击吸收功

Fig. 3 Impact absorption energy at serial temperature at E=10 kJ/cm

2.2 组织结构特征及其对性能的影响

现代管线钢是一种控轧、控冷状态的低碳微合金化钢. 由于低碳、超低碳和多元的微合金化设计,以及在焊接过程中加热速度快、加热温度高和冷却速度范围较广的工艺特点,管线钢焊接粗晶热影响区(CGHAZ)的显微组织形态呈现多样性和复杂性[6].

X100管线钢母材典型的光学显微组织为针状铁素体. 在 TEM下,这种针状铁素体的形态如图 4

由平行的板条贝氏体铁素体组成，板条间分布有 M-A组元.

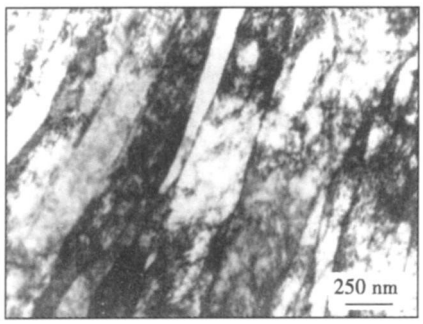

图 4　X100母材的透射电镜组织

Fig. 4　TEM microstructure of X100 base steel

具有针状铁素体特征的这种 X100管线钢在经受不同焊接参数的热过程后，其显微组织发生较大的变化. 图 5是在不同的焊接热输入下，X100焊接粗晶热影响区的光学显微组织. 已有的研究结果表明[7]，在管线钢的焊接热过程中，根据焊接热输入不同，所形成的主要组织形态主要有多边形铁素体（PF）、准多边形铁素体（QF）、粒状贝氏体（GB）和贝氏体铁素体（BF）.

图 5a表明，在较低的焊接热输入下（10 kJ/cm），由于冷却速度较大，CGHAZ的组织形态多为从奥氏体晶界向晶内平行生长的细密板条，不同位向的板条使原奥氏体晶界清晰可见. 分析表明，这种细密的板条组织为 BF+GB，板条间为薄膜状

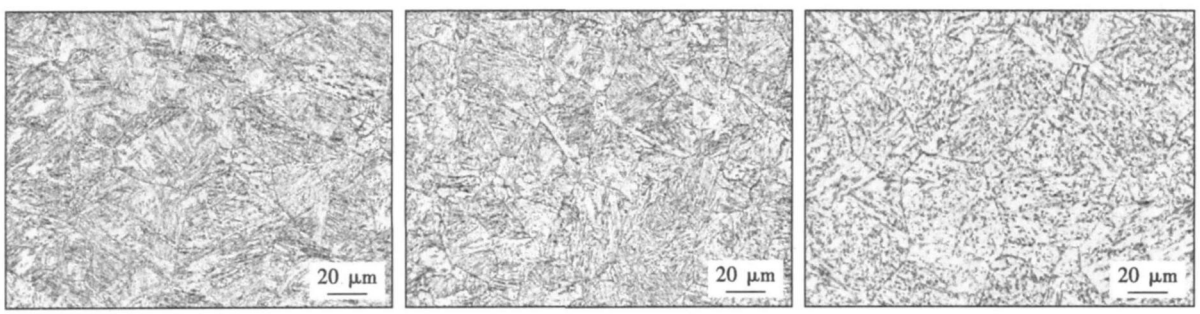

图 5　X100在不同焊接热输入下的光学显微组织

Fig. 5　OM microstructure of X100 at different welding inputs

或条状 M-A组织较为细小. 这种 BF+GB的 SEM和 TEM的电子显微形态如图 6所示. 这一组织形态所具有的细小的有效晶粒、高密度的位错亚结构和弥散分布的微合金碳、氮化合物的沉淀析出等组织结构因素，赋予材料优良的强韧特性[8].

在中等焊接热输入下（20 kJ/cm），管线钢 CGHAZ组织形态有所不同. 由图 5b可以看出，由于冷速有所降低，CGHAZ的组织主要为 GB+QF. 这种组织形态的 SEM形貌如图 7所示. 比较图 6和图 7可以发现，在图 6的快冷条件下，板条细小，板条间的岛状组织纵横比较大，并由这种岛状组织勾画出板条的痕迹. 而在图 7的较慢冷却速度下，这种岛状组织多呈块状，并出现部分 QF，因而使得 CGHAZ的强韧性有所降低.

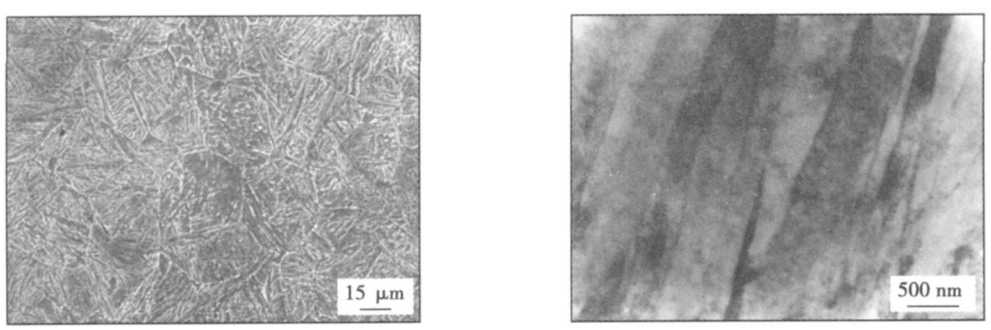

图 6　E= 10 kJ/cm时的组织

Fig. 6　Microstructure at E= 10 kJ/cm

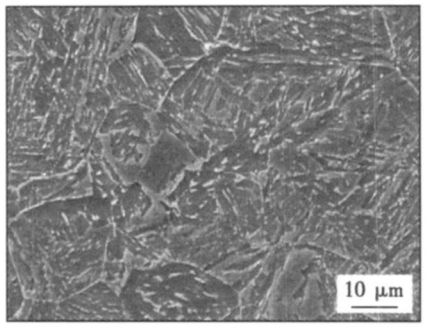

图 7 E=20 kJ/cm时的扫描电镜形貌
Fig. 7 SEM morphology at E=20 kJ/cm

在高的焊接热输入下（50 kJ/cm），由于冷却速度的降低，管线钢的组织形态发生了明显的变化．由图 5 c的组织观察可以发现：一方面，晶粒粗化的倾向比较明显；另一方面，组织中的 QF+PF增多．在 TEM下（图 8），这种多边形铁素体或等轴铁素体的组织特征揭示得更为清晰．一般认为[7]，多边形铁素体不是管线钢的理想组织状态．随着多边形铁素体或等轴铁素体组织含量的增加，材料的强韧性降低．

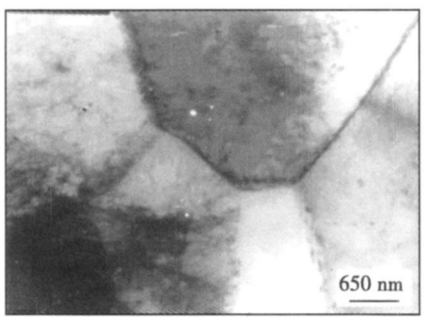

图 8 E=50 kJ/cm时形成的多边形铁素体
Fig. 8 PF at E=50 kJ/cm

3 结 论

（1）随着焊接热输入的增加，X100管线钢的强韧性降低．当焊接热输入在 10～20 kJ/cm范围内，X100管线钢的焊接粗晶热影响区有较好的强韧特性，可作为 X100管线钢推荐的热输入．

（2）在 10 kJ/cm左右的较低热输入下，X100管线钢焊接粗晶热影响区的显微组织为 BF+GB，这种组织赋予材料以最佳的强韧性水平．

（3）在 20 kJ/cm左右的中等焊接热输入下，X100管线钢焊接粗晶热影响区的显微组织以 GB+QF为主，材料有较好的强韧配合．

（4）当热输入为 50 kJ/cm时，一方面晶粒粗化比较明显，另一方面粗晶区中的 BF和 GB被 QF和 PF替代，致使材料的强韧性降低．

参考文献：

[1] Okaguchi S. Production and development of X100 and X120 grade line pipes[C] // Beijing: International Seminar Forum of X100/X120 Grate High Performance Pipe Steels, 2005.

[2] 罗海文，董 瀚. 高级别管线钢 X80－X120的研发与应用[J]. 中国冶金，2006，16(4)：14－15.
Luo Haiwen, Dong Han. Development of X80－X120 high grade linepipe steels and their applications[J]. China Metallurgy, 2006, 16(4): 14－15.

[3] Glover A. Research and application of X100 and X120[C] // Beijing: Proceedings of Symposium on X80 Grade Steel and Line pipes, 2004.

[4] Takeuchi J. Development and evaluation of high strength linepipe for high pressure gas transmmison pipeline[C] // Xi'an: International Seminar on Application of High Strength Line Pipe, 2006.

[5] 郑 磊，傅俊岩. 高等级管线钢的发展现状[J]. 钢铁，2006，41(10)：1－10.
Zheng Lei, Fu Junyan. Recent development of high performance pipeline steel[J]. Steel & Iron, 2006, 41(10): 1－10.

[6] 高惠临. 管线钢——组织 性能 焊接行为[M]. 西安：陕西科学技术出版社，1995.

[7] 冯耀荣，高惠临，霍春勇，等. 管线钢显微组织的分析与鉴别[M]. 西安：陕西科学技术出版社，2008.

[8] 李鹤林，郭生武，冯耀荣，等. 高强度微合金管线钢显微组织分析与鉴别图谱[M]. 北京：石油工业出版社，2001.

作者简介：张骁勇，男，1971年出生，博士研究生．主要从事管线钢的研究和教学工作．发表论文 10余篇．
Email: xyzhang@xsyu.edu.cn

Abstract: The effects of welding speed and welding direction on Nd: YAG laser-short current MAG hybrid welding stability were investigated. The experimental results showed that welding arc stability of MAG and laser+MAG would decrease with the increasing of welding speed, but the arc of laser+MAG get more stable comparing with MAG arc. The maximal welding speed of laser+MAG is more than one time fast comparing with that of MAG. The hybrid welding arc in arc leading direction would get more stable comparing with that of laser leading direction.

Key words: GMAW; laser welding; hybrid welding; welding process stability

Analysis of laser-MAG hybrid welding plasma radiation

LI Zhiyong, WANG Wei, WANG Xuyou, LI Huan (1. Welding Research Center, North University of China, Taiyuan 100081, China; 2. Harbin Welding Institute, Harbin 150080, China; 3. School of Material Science and Engineering, Tianjin University, Tianjin 300072, China). p 21—24, 28

Abstract: Hollow probe is used to detect the plasma radiation of specific point passing the probe for spectrum collecting. The radiation of MAG and laser-MAG hybrid welding are collected with fiber spectrometer. The spatial distribution of the radiation is analyzed to compare the differences between welding process with and without laser hybrid. Furthermore, high speed video is also applied to study the coupling mechanics of laser-MAG hybrid. The result shows that a higher radiation intensity zone will be formed in the arc center. Beside the center zone, there is a somewhat lower radiation intensity zone. An ionized duct zone will be formed near the laser focused point. The ionized duct is dominated by Fe fume. The ionized duct makes the welding arc more stable when the laser is applied. The higher radiation intensity zone changes the distribution of plasma energy, thus makes the energy focus on the arc center. The coupling effect of laser-MAG hybrid welding will form weld bead with deeper penetration than MAG welding.

Key words: laser; MAG; hybrid welding; plasma; spectrum

Feature evaluation and selection of penetration arc sound signal based on neural network

LIU Lijun, LAN Hui, ZHENG Hongyan (1. Ningbo Institute of Technology, Zhejiang University, Ningbo 315100, Zhejiang, China; 2. School of Material Science & Engineering, Harbin University of Science and Technology, Harbin 150080, China; 3. Applied Science College, Harbin University of Science and Technology, Harbin 150080, China). p 25—28

Abstract: In welding processing, penetration detection and diagnosis based on arc sound, how to choose its proper parameters is vital to diagnosis. The feature evaluation and selection methods were presented, the results trained by neural network were used to evaluate feature parameters. Because neural network satisfied the nonlinear mapping requirement for high-resolution information compression, the complex classification problem in welding penetration pattern recognition was transferred to feature processing stage, and feature extration was realized by neural network effectively. An illustration validated the effectiveness of the method.

Key words: neural network; penetration; arc sound; feature evaluation; pattern recognition

Influence of welding heat input on microstructure and properties of coarse grain heat-affected zone in X100 pipeline steel

ZHANG Xiaoyong, GAO Huilin, ZHUANG Chuanjing, JI Lingkang (1. School of Materials Science and Engineering, Xi'an University of Architecture and Technology, Xi'an 710055, China; 2. School of Materials Science and Engineering, Xi'an Shiyou University, Xi'an 710065, China; 3. Tubular Goods Research Center of China National Petroleum Corporation, Xi'an 710065, China). p 29—32

Abstract: The influence of welding heat input on the microstructure characterization and properties of coarse grain heat-affected zone (CGHAZ) in a X100 pipeline steel were investigated by means of thermal simulation technique, microscopic analysis method and mechanical property testing. The results showed that the strength and toughness of X100 pipeline steel decreased with the welding heat input increasing. The microstructure of CGHAZ was mainly made up of bainitic ferrit and granular bainitic which could bring excellent strength and toughness when welding heat was about 10 kJ/cm. The quasi-polygonal ferrite and granular bainitic were formed with welding heat input about 20 kJ/cm, which could get fine strength-toughness. When the welding heat input was higher than 30 kJ/cm, the strength and toughness decreased because of the increasing of polygonal ferrite. Therefore, welding heat input at range of 10—20 kJ/cm was recommended in the welding process of X100 pipeline steels.

Key words: X100 pipeline steel; welding heat input; microstructure; properties

Establish of ultrasonic residual stress measurement system based on entire envelope weighting algorithm

WU Zhonghua, ZHANG Shiping, SUN Haoyu, ZHU Zheng (1. College of Mechanical and Electronic Engineering, China University of Petroleum, Dongying 257061, Shandong, China; 2. Drilling Technology Research Institute, Shengli Petroleum Administration Bureau, Dongying 257017, Shandong, China; 3. School of Electrical Engineering and Automatic, Harbin Institute of Technology, Harbin 150001, China). p 33—36

Abstract: The entire envelope weighting algorithm is proposed in this paper and realized by virtual instrument to obtain residual stress by ultrasonic measurement. Different weight of reference point is assigned to measure time of echo signal more accurately. Compared with traditional single threshold method, the experiment results show that the algorithm improved the stabilization of repeat measurement at the same point by different conditions. The uncertainty is calculated to validate the accuracy of the ultrasonic measurement.

Key words: ultrasonic measurement; welding residual stress; weighting algorithm

High gradient residual stresses during laser deep penetration welding of titanium alloy

ZHANG Kerong, ZHANG Jianxun (School of Materials Science & Engineering, Xi'an Jiaotong